

2 Geometrical Correlation Project

– in quest for the origin of heavy fermion behavior in *d*-electron systems –

Project Leader: Ryosuke Kadono

2-1 Introduction

Geometrical frustration in electronic degrees of freedom such as spin, charge, and orbit, which is often realized in the stages of highly symmetric crystals, has been one of the major topics in the field of condensed matter physics. In particular, the heavy fermion (HF) behavior in $Y_{1-x}Sc_xMn_2$ [$Y(Sc)Mn_2$] [1, 2] and LiV_2O_4 [3, 4] has attracted broad interest, where such a local electronic correlation specific to the highly symmetric pyrochlore structure may be of direct relevance to the formation of the heavy quasiparticle (QP) state. However, despite decades of studies, the microscopic mechanism by which the local correlation is transformed into the heavy QP mass of itinerant *d*-electrons in these compounds still remains controversial.

In general, the development of heavy QPs accompanies narrowing of the effective band width (W) or an increase in the density of states (DOS) at the Fermi energy [$D(E_F)$]. It is thus expected from a naive consideration based on Heisenberg's uncertainty principle that the HF behavior should manifest itself in the spin dynamics as reduction of the spin fluctuation rate (ν) because these quantities are mutually linked by the following relation:

$$\nu \sim \frac{W}{\hbar} \simeq \frac{1}{\hbar D(E_F)}. \quad (1)$$

Since the effective QP mass is directly connected to the DOS via the relation $m^* \propto [D(E_F)]^{2/3}$ for a three-dimensional (3D) Fermi gas, studies on the spin fluctuation with particular emphasis on relatively low energies should provide valuable information on the mechanism of heavy QP formation.

As a probe of spin fluctuation, muon spin

rotation (μ SR) has a unique frequency window with high sensitivity for $10^5 \leq \nu \leq 10^{11} \text{ s}^{-1}$, filling the gap between those covered by nuclear magnetic resonance (NMR) and neutron scattering. This provides promising perspectives for the μ SR study of *d*-electron HF-like compounds. Here, we establish that the longitudinal spin relaxation rate ($\lambda \equiv 1/T_1$) in the above-mentioned compounds exhibits a common feature that it asymptotically becomes independent of temperature upon cooling below a crossover temperature of $T^* \simeq 10^1\text{--}10^2$ K. This, within the framework of fermionic QPs, means that the spin fluctuation rate becomes linearly dependent on temperature, $\nu \propto T$, which is in marked contrast to ordinary metals, where ν is independent of T as determined by the DOS at the Fermi level. Considering that the transition-metal ions in these compounds comprise a pyrochlore lattice, it is naturally expected that the above-mentioned feature in the spin dynamics will be specific to the relevant lattice structure. We argue that this is indeed the case in that the underlying spin dynamics can be understood by the spin correlation of the intersecting Hubbard chains, which provides a model of the pyrochlore lattice. This strongly indicates the crucial role of t_{2g} bands that preserve the one-dimensional (1D) character specific to the undistorted pyrochlore lattice at low energies, which is consistent with a theoretical scenario that the 1D-3D crossover due to coupling between these 1D chains developing at low temperatures is the origin of the HF behavior.

In the following, we present an overview of our work for $Y(Sc)Mn_2$ [5], $YMn_2Zn_{20-x}In_x$ [6], and LiV_2O_4 [7, 8], conducted over the past six years under "Geometrical Correlation Project". Although the results quoted in this review are

mostly concerned with those obtained from μ SR studies [9], they are supported by collaborations with experts on other quantum beam techniques including synchrotron radiation and neutron gathered in the Condensed Matter Research Center serving as a COE of “multiprobe” researches.

The structure of this review is as follows. For sorting out the technical matter, an introduction to the muon spin rotation will be presented with the primary focus on the longitudinal spin relaxation rate (λ) and the physical quantities extracted thereof. Then, the temperature dependence of λ and the associated spin fluctuation rate in the abovementioned compounds is discussed in connection with a possible scenario for the origin of heavy QPs in these compounds. We also show that the anomalous behavior of λ is accompanied by strong broadening of the linewidth under a transverse field ($\lambda_{\perp} \equiv 1/T_2$), which is not explained by the hyperfine parameters extrapolated from their values at high temperatures [10, 11].

2-2 Muon Spin Relaxation in Itinerant Electron Systems

As a probe of spin fluctuation in condensed matter, μ SR is kin to NMR, primarily because of the fact that an implanted muon can be regarded as a light radioisotope of a proton (^1H). Nonetheless, while the physics behind the mechanism of spin relaxation is common, there are two major factors, i.e., the time windows of observation (10^{-4} – 10^0 s for NMR, 10^{-9} – 10^{-5} s for μ SR) and the relevant sites (on-site for NMR, interstitial site for μ SR), that make these two techniques distinct (or even complementary with each other). It would be useful to highlight such differences by examining the longitudinal spin relaxation rate ($1/T_1$) in simple metals.

According to Korringa’s relation, the spin relaxation induced by s band electrons is given by

$$T_1 T K_s^2 = \frac{\hbar}{4\pi k_B} \left(\frac{\gamma_e}{\gamma_{\mu}} \right)^2, \quad (2)$$

where $\gamma_e (= 2\pi \times 28024 \text{ MHz})$ and $\gamma_{\mu} (= 2\pi \times 135.53 \text{ MHz})$ are the respective gyromagnetic ratios of an electron and muon. K_s is the Knight shift, which is expressed in terms of the hyperfine field (H_s) per electron as

$$K_s = \frac{H_s}{N_A \mu_B} \chi_p, \quad (3)$$

N_A is Avogadro’s number, μ_B is the Bohr magneton, and χ_p is the magnetic susceptibility [$\chi_p = 2\mu_B^2 D(E_F)$ for uncorrelated electrons]. Equation (2) may be rewritten as

$$\lambda \equiv \frac{1}{T_1} = \frac{4\pi}{\hbar} (\hbar\gamma_{\mu} H_{\alpha})^2 \left[\frac{D_{\alpha}(E_F)}{N_A} \right]^2 k_B T, \quad (4)$$

where H_{α} is the hyperfine field of electrons at α orbitals ($\alpha = s, p, d, \dots$) with $D_{\alpha}(E_F)$ denoting the DOS for the corresponding band.

Here, let us consider the example of pure silver (Ag), in which the muon Knight shift has been reported to be $K_s = 94(3.5) \text{ ppm}$ [12]. Equation (2) then yields

$$T_1 T = \frac{T}{\lambda} \simeq 2.94 [\text{K} \cdot \text{s}].$$

A similar estimation for silver nuclei (e.g., ^{107}Ag , where $K_s \simeq 0.52\%$) leads to $T_1 T \simeq 5.93 [\text{K} \cdot \text{s}]$, which is comparable to the $T_1 T$ value for muon. Considering the melting point of silver ($\simeq 10^3 \text{ K}$), it implies that $1/T_1 \leq 10^3 \text{ s}^{-1}$, which is far below the sensitive range for μ SR, while it is readily observed by NMR. Thus, the s band electron makes a negligible contribution to $1/T_1$ in μ SR.

When the electronic correlation is not negligible, it is useful to resort to a more general form of $1/T_1$ with the relevant spin fluctuation expressed by spin density operators,

$$\lambda = \gamma_{\mu}^2 \sum_q A_q A_{-q} \int_{-\infty}^{\infty} dt \cos \omega_{\mu} t \frac{\langle [S_q^+(t), S_{-q}^-(0)] \rangle}{2}, \quad (5)$$

where $\omega_{\mu} = \gamma_{\mu} B_0$ (B_0 being the external field) and A_q and S_q^{\pm} are the Fourier components of the hyperfine field [$A_{\mu}(r)$] and spin density [$S_q^+ = \sum_{\mathbf{k}} c_{\mathbf{k}+\mathbf{q},\uparrow}^* c_{\mathbf{k},\downarrow}$, $S_q^- = \sum_{\mathbf{k}} c_{\mathbf{k}+\mathbf{q},\downarrow}^* c_{\mathbf{k},\uparrow}$, with $c_{\mathbf{k},\uparrow}^*/c_{\mathbf{k},\downarrow}$ being the creation/annihilation operators for spin up(\uparrow)/down(\downarrow) electrons], respectively, [A, B] = $\frac{1}{2}(AB+BA)$, and $\langle Q \rangle = \text{Tr}[e^{-(H'/k_B T)} Q] / \text{Tr}[e^{-(H'/k_B T)}]$ (with H' being the Hamiltonian of the electron system) [13]. Imposing the fluctuation-dissipation theorem, which links the thermal fluctuation described by the correlation function to the imaginary part (dissipation) of the generalized susceptibility,

$$\frac{2\hbar\chi_{\perp}''(\mathbf{q}, \omega_{\mu})}{N_A \mu_B^2 (1 - e^{-\hbar\omega_{\mu}/k_B T})} = \int_{-\infty}^{\infty} dt \cos \omega_{\mu} t \frac{\langle [S_q^+(t), S_{-q}^-(0)] \rangle}{2}, \quad (6)$$

to Eq. (5) with the further assumption that $\hbar\omega_{\mu} \ll k_B T$ leads to

$$\lambda \simeq \frac{2\gamma_\mu^2}{N_A\mu_B^2} k_B T \sum_{\mathbf{q}} A_{\mathbf{q}} A_{-\mathbf{q}} \frac{\chi''_{\perp}(\mathbf{q}, \omega_\mu)}{\omega_\mu}, \quad (7)$$

where $\chi''_{\perp}(\mathbf{q}, \omega_\mu)$ is the imaginary part of the dynamical spin susceptibility (perpendicular to the quantization axis that is usually determined by B_0).

The actual form of $A_{\mathbf{q}}$ is determined by $A_\mu(\mathbf{r})$ (with $\mathbf{r}=0$ at the muon position), and thus it generally depends on the muon site(s). An exception is the case that the hyperfine field is predominantly determined by the Fermi contact interaction, $A_\mu(\mathbf{r}) \simeq A_\mu \cdot \delta(\mathbf{r})$, so that $A_{\mathbf{q}} = A_\mu$ irrespective of \mathbf{q} . Equation (7) is then reduced to

$$\lambda \simeq \frac{2\gamma_\mu^2}{N_A\mu_B^2} k_B T A_\mu^2 \sum_{\mathbf{q}} \frac{\chi''_{\perp}(\mathbf{q}, \omega_\mu)}{\omega_\mu}. \quad (8)$$

However, such a situation is rare for μ SR because of the small charge of a muon (same as that of a proton) and the fact that muons are usually located at the interstitial sites. Consequently, the magnetic dipolar interaction is the primary source of hyperfine fields acting on muons,

$$\hat{A}_\mu(\mathbf{r}) = A^{\alpha\beta}(\mathbf{r}) = \sum_j \frac{1}{r_j^3} \left(\frac{3\alpha_j\beta_j}{r_j^2} - \delta_{\alpha\beta} \right) (\alpha, \beta = x, y, z), \quad (9)$$

where $\mathbf{r}_j = (x_j, y_j, z_j) = \mathbf{R}_j - \mathbf{r}$ with \mathbf{R}_j being the position of the j th electron. More specifically, the effective hyperfine field in the paramagnetic state is given by the second moment

$$\hat{A}_\mu^2(\mathbf{r}) = \sum_{\alpha, \beta} [A^{\alpha\beta}(\mathbf{r})]^2, \quad (10)$$

where the corresponding Fourier transform ($A_{\mathbf{q}}^{\alpha\beta}$)² can be numerically evaluated for the specific muon site(s). An example calculated for $\mathbf{q} \parallel [110]$ in Y(Sc)Mn₂ is shown in Fig. 1(b), where the muon is presumed to be at the 16c site [see Fig. 1(a)]. It shows a broad distribution with a peak near $\mathbf{q} \simeq 0$ and a tail over the region $|\mathbf{q}| \leq \sim 1\text{\AA}^{-1}$. A similar result is observed for the [1-10] direction, indicating that Eq. (7) can be approximated by the form

$$\lambda \simeq \frac{2\gamma_\mu^2}{N_A\mu_B^2} k_B T \sum_{\alpha=x,y; \beta=x,y,z} \left(A_{\mathbf{q}=0}^{\alpha\beta} \right)^2 \frac{\chi''_{\perp}(\mathbf{q} \simeq 0, \omega_\mu)}{\omega_\mu}. \quad (11)$$

Following the assumption generally adopted in NMR (that the density spectrum of spin fluctuation is described by the Lorentzian distribution function $f(\omega)$ with its amplitude represented by the local susceptibility χ ,

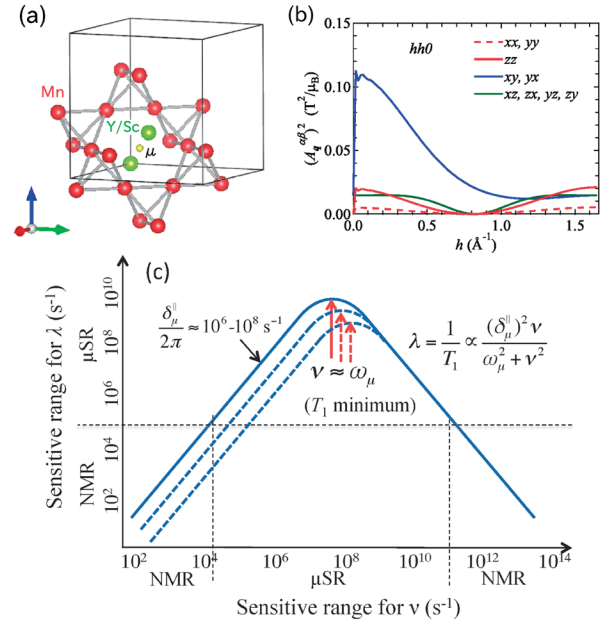


Fig. 1: (a) Crystal structure of Y(Sc)Mn₂, where Y/Sc and Mn atoms are indicated by green and red spheres, respectively. Mn atoms form a network of corner-shared tetrahedra known as a pyrochlore lattice. A small yellow circle shows the 16c site presumed to be occupied by implanted muons. (b) Fourier transform of the hyperfine field distribution $\hat{A}_\mu^2(\mathbf{r})$ in Y(Sc)Mn₂ with a 16c site at the origin. (c) Sensitive range of spin fluctuation rate for μ SR and NMR predicted from Eq. (13), where the hyperfine field is presumed to be 10^{-2} – 10^0 T. Note that the sensitive ranges for NMR are split into two different ranges, where the high-frequency range corresponds to the region close to the limit of motional narrowing. Dashed curves show λ for greater external magnetic fields ($\propto \omega_\mu$).

$$\frac{\chi''_{\perp}(\mathbf{q} \simeq 0, \omega_\mu)}{\omega_\mu} \simeq \chi \cdot f(\omega_\mu) = \chi \frac{\nu}{\nu^2 + \omega_\mu^2}, \quad (12)$$

Eq. (11) is further simplified to

$$\lambda(\nu, \omega_\mu) \simeq \frac{k_B T \chi}{N_A \mu_B^2} \cdot \frac{(\delta_\mu^{\parallel})^2 \nu}{\nu^2 + \omega_\mu^2}, \quad (13)$$

where δ_μ^{\parallel} is the redefined hyperfine parameter and ν is the fluctuation rate of δ_μ^{\parallel} at $\mathbf{q} \simeq 0$. The above equation is valid when $\nu \gg \delta_\mu^{\parallel}$. Equation (12) corresponds to the general assumption in the time domain that the correlation of a fluctuating hyperfine field can be described by the stationary Gaussian–Markovian process in the approximated form

$$\langle A_\mu(t_0) A_\mu(t_0 + t) \rangle = \langle A_\mu^2 \rangle \exp(-\nu|t|). \quad (14)$$

While μ SR and NMR can be used to observe the spin fluctuation via the same process described by Eq. (13), their sensitive ranges

are markedly different (as already discussed in the case of s band electrons). As illustrated in Fig. 1(c), the difference stems from the sensitive range of λ ($= 1/T_1$), which is determined by the accessible time window, T_w , for the respective probes (see also Table I). The present study benefits greatly from this unique sensitive range of μ SR to spin fluctuation. We rely on Eq. (13) to deduce ν explicitly from the experimentally determined longitudinal spin relaxation rate λ .

	μ SR	NMR
Time window(T_w)	$10^{-9} \leq T_w \leq 10^{-5}$ [s]	$10^{-4} \leq T_w \leq 10^1$ [s]
Fluctuation rate(ν)	$10^4 \leq \nu \leq 10^{11}$ [s $^{-1}$]	$\nu \leq 10^4, \nu \geq 10^{11}$ [s $^{-1}$]

Table I: Sensitive ranges of spin fluctuation rate for μ SR and NMR predicted from Eq. (13). See Fig. 1(c) for more details.

2-3 Overview of μ SR Results

2-3-1 Y(Sc)Mn $_2$

Yttrium manganite (YMn $_2$) is an intermetallic Laves phase (C15-type) compound and was the first transition-metal system in which HF behavior was observed. As shown in Fig. 1, it comprises a 3D network of corner-shared tetrahedra with Mn ions at their corners, resulting in a scheme equivalent to a cubic pyrochlore lattice. Although YMn $_2$ exhibits magnetic order with complex helical modulation and a large volume expansion below $T_N \approx 100$ K [14], it remains in the paramagnetic state under hydrostatic pressure (≥ 0.4 GPa) or upon the substitution of Y by Sc (Y $_{1-x}$ Sc $_x$ Mn $_2$, with $x \geq 0.03$), which is also accompanied by a large increase in the QP mass ($m^* \approx 15$ times the band mass) as inferred from the electronic specific heat [2].

Our μ SR measurements were performed using polycrystalline samples of Y $_{1-x}$ Sc $_x$ Mn $_2$ with various Sc contents ($x = 0.03, 0.05, 0.07$, and 0.08 , as prepared) grown from melts in an argon arc furnace followed by annealing, where the details of sample preparation are described elsewhere. The bulk properties of these samples including the electronic specific heat (Sommerfeld) coefficient and uniform spin susceptibility (χ) were in good agreement with earlier reports (see Ref. [5] for more details).

Figure 2 shows some examples of time-dependent μ SR spectra at a low temperature (≈ 2 K), where pairs of spectra obtained at two different longitudinal fields (LF, 10mT and 5T) are displayed for comparison [5]. The depolarization

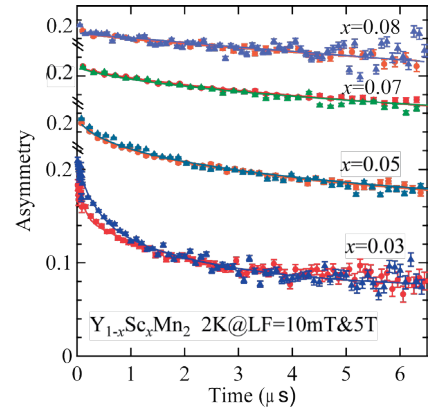


Fig. 2: Typical examples of μ SR spectra [time-dependent asymmetry, $A(t)$] observed for Y(Sc)Mn $_2$ at 2 K under two different longitudinal fields [$B_0 = 10$ mT (circles) and 5 T (triangles)], where spectra for $x \geq 0.05$ are shifted vertically by 0.05 with each x for clarity. Solid curves show best fits using the function described in the text. Those for $x = 0.03$ exhibit a slight dependence on B_0 , from which the hyperfine parameter is estimated, whereas the spectra are less dependent on B_0 for $x \geq 0.05$.

rate (λ) decreases with increasing Sc content x and tends to approach an asymptotic value (as it exhibits little change between $x = 0.07$ and 0.08). It is also noticeable that λ is mostly independent of the magnitude of the longitudinal field (B_0) for $x \geq 0.05$, while it shows a slight variation with B_0 for $x = 0.03$. These features can be readily understood from Eq. (13) introduced in the previous section. We also note that Eq. (13) has been successfully applied to various types of magnetism including that of quasi-1D compounds [16]. Equation (13) is modified to yield the fluctuation rate

$$\nu \approx \frac{(\delta_\mu^\parallel)^2 k_B T \chi}{2N_A \mu_B^2 \lambda} \pm \left[\left(\frac{(\delta_\mu^\parallel)^2 k_B T \chi}{2N_A \mu_B^2 \lambda} \right)^2 - \omega_\mu^2 \right]^{1/2}$$

from the experimental values of λ and χ , where the double sign corresponds to the two cases of $\nu > \omega_\mu$ (+) and $\nu < \omega_\mu$ (-) [see Fig. 1(c)]. The fact that the spectra in Fig. 2 are mostly independent of ω_μ indicates that $\nu \gg \omega_\mu$, from which Eq. (13) is reduced to yield

$$\nu \approx \frac{(\delta_\mu^\parallel)^2 k_B T \chi}{N_A \mu_B^2 \lambda}. \quad (15)$$

The magnitude of δ_μ^\parallel was determined as the gradient of the muon Knight shift (K) plotted against susceptibility (i.e., $dK/d\chi$ in the K - χ plot), for which additional μ SR measurements under a high transverse field (HTF) were performed on freshly synthesized samples with $x = 0.05, 0.07$, and 0.09 . [11] The fast Fourier transforms (FFTs)

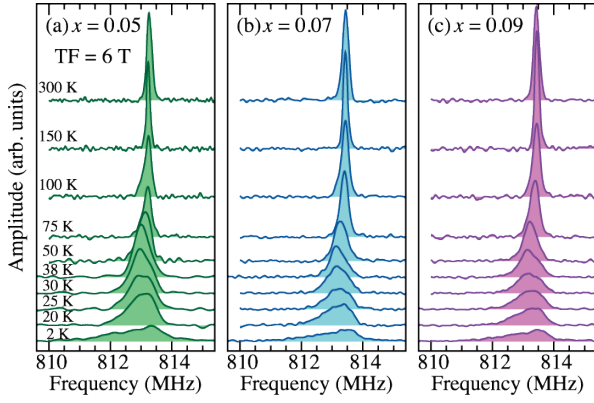


Fig. 3: FFTs of μ SR spectra observed at various temperatures for $Y_{1-x}Sc_xMn_2$ with (a) $x = 0.05$, (b) 0.07, and (c) 0.09.

of the HTF- μ SR spectra observed for these samples at various temperatures are shown in Fig. 3. These spectra can be used to monitor the density distribution of the local internal field at the muon site [$P(\omega_\mu)$] via the relation

$$\omega_\mu = \omega_0 + \gamma_\mu B_{\text{loc}}, \quad (16)$$

where B_{loc} is the local field from nearby electrons. The second moment of the local field distribution parallel to B_0 is directly related to the corresponding hyperfine parameter δ_μ ($\equiv \delta_\mu^\perp$) as

$$\delta_\mu^2 = \frac{1}{2} (\delta_\mu^\parallel)^2 \propto \overline{\gamma_\mu^2 (B_{\text{loc}}^\parallel)^2} \quad (17)$$

in the case of isotropic hyperfine fields, where $(B_{\text{loc}}^\parallel)$ is the component of B_{loc} parallel to B_0 and the overline denotes the mean value. The transverse relaxation rate is then given by

$$\lambda_\perp \simeq \left[\frac{2\delta_\mu^2 \nu}{\nu^2 + \omega_\mu^2} + \frac{\delta_\mu^2}{\nu} \right] \cdot \frac{k_B T \chi}{N_A \mu_B^2}. \quad (18)$$

It is noticeable that the spectra become broad and asymmetric with decreasing T below $T^* \sim 100$ K, which seems in accordance with the onset of the Curie–Weiss behavior of χ (see Fig. 4 inset). The magnitude of the linewidth ($\lambda_\perp \simeq 2\text{--}5$ MHz at 2 K) is much greater than that expected from Eq. (18) with δ_μ determined by $dK/d\chi$. Such broadening was also reported in the cases of LiV_2O_4 [10] and $\text{YMn}_2\text{Zn}_{20-x}\text{In}_x$ (see below). The nearly identical linewidth for different Sc contents x shown in Fig. 3 indicates that the broadening at lower temperatures is not due to extrinsic effects such as crystallographic randomness owing to the Sc substitution or the formation of a spin-glass

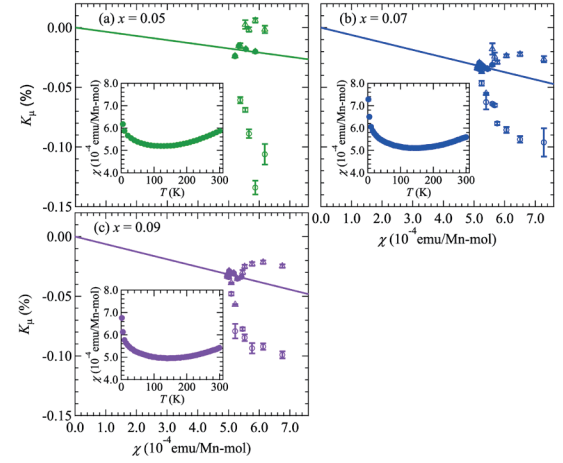


Fig. 4: K - χ plots obtained for $Y(\text{Sc})\text{Mn}_2$ with (a) $x = 0.05$, (b) 0.07, and (c) 0.09, where the solid lines are the results of curve fitting for the data above $T^* \sim 100$ K. Inset: temperature dependence of magnetic susceptibility (χ) used in the K - χ plot.

state observed for a smaller Sc content[17]. As is discussed in Sect., we attribute this broadening to the strong spin fluctuation associated with geometrical frustration.

Curve fitting of these spectra using the form

$$AG_x(t) = A_0 \sum_{i=1}^m \exp(-\lambda_\perp^{(i)} t) \cos(\omega_\mu^{(i)} t + \phi_0) \quad (19)$$

yielded reasonable agreement with data for $T \geq T^*$ assuming one frequency component ($m = 1$), where A_0 is the initial asymmetry, λ_\perp is the transverse spin depolarization rate, and ϕ_0 is the initial phase. The Knight shift was then determined by

$$K_i = \frac{\omega_\mu^{(i)} - \omega_0}{\omega_0} \quad (20)$$

where ω_0 was determined by additional measurements on a reference sample of high purity silver. Meanwhile, two frequency components ($m = 2$) were incorporated to obtain satisfactory fits for the data below T^* .

Some examples of K - χ plots are shown in Fig. 4[11]. Considering the line broadening at lower temperatures, the hyperfine parameters are deduced from $dK/d\chi$ for $T \geq T^*$ to yield $\delta_\mu/2\pi = -26(3)$ MHz/ μ_B ($x = 0.05$), $-47(1)$ MHz/ μ_B ($x = 0.07$), and $-49(1)$ MHz/ μ_B ($x = 0.09$), where the scattering among different x is probably due to the residual influence of the line broadening (note that the relative variation of K and χ is small for the relevant temperature region). However, their mean value [$\delta_\mu/2\pi = -41(2)$ MHz/ μ_B] is in perfect

agreement with the calculated value assuming that muons are located at the 16c site [17, 18], $|\delta_\mu/2\pi\mu_B| = 40.2 \text{ MHz}/\mu_B$. Although it is inferred from the ^1H NMR of YMn_2 that the hydrogen site is the 96g site, which is slightly away from the 16c site [19], the calculated value of the muon hyperfine parameter ($\delta_\mu/2\pi = 78.6 \text{ MHz}/\mu_B$) makes it unlikely that a muon occupies this site.

The LF- μSR time spectra in Fig. 2 were analyzed by least-squares curve fitting to deduce λ using

$$AG_z(t) = A_0 G_z^{\text{KT}}(t) \cdot [(1 - a_p)\exp\{-(\lambda t)^\beta\} + a_p] \quad (21)$$

$$\approx [(1 - a_p)\exp\{-(\lambda t)^\beta\} + a_p], \quad (22)$$

where $G_z^{\text{KT}}(t)$ is the Kubo-Toyabe relaxation function, which is approximated by $G_z^{\text{KT}}(t) \approx 1$ for high B_0 , β is the power, and a_p is a constant term. Here, we introduce stretched exponential decay ($\beta \neq 1$) to reproduce the deviation of the spin dynamics from that described by the model of spin correlation with a single value of δ_μ^\parallel and/or ν at a given temperature [17, 20]. The presence of the term a_p is clearly inferred in the case of $x = 0.03$ from the leveling off of the time spectra for $t \geq 4 \mu\text{s}$ (see Fig. 2; as is also needed for $x = 0.05$). It is presumed that these deviations from single exponential decay are related to the strong line broadening observed under a transverse field. Apart from this ambiguity, excellent fits were obtained in all of the cases with a_p fixed to the values deduced at 2 K. The solid curves in Fig. 2 represent the best fits obtained under these conditions [5].

The temperature dependences of the parameters deduced by curve fitting are summarized in Fig. 5. Although β varies only slightly with x , λ exhibits a clear tendency of becoming less dependent on temperature, i.e.,

$$\lambda = \frac{1}{T_1} \propto T^0 (T \leq T^*), \quad (23)$$

with increasing x . Considering the dependence of λ on ν and χ in Eq. (13), this means that ν becomes linearly dependent on T with increasing x . Meanwhile, the behavior of λ for $x \rightarrow 0.03$ is understood as the freezing of the Mn spin fluctuation because the transition to the quasistatic spin-glass state occurs in the sample with $x = 0.03$ below $T_g \approx 3 \text{ K}$ (where T_g is defined as the peak muon depolarization rate under $B_0 = 10 \text{ mT}$) [17]. The behavior of λ observed for $x \geq 0.07$ shows a distinct similarity to that for LiV_2O_4 [7].

As shown in Fig. 6, the spin fluctuation rate in

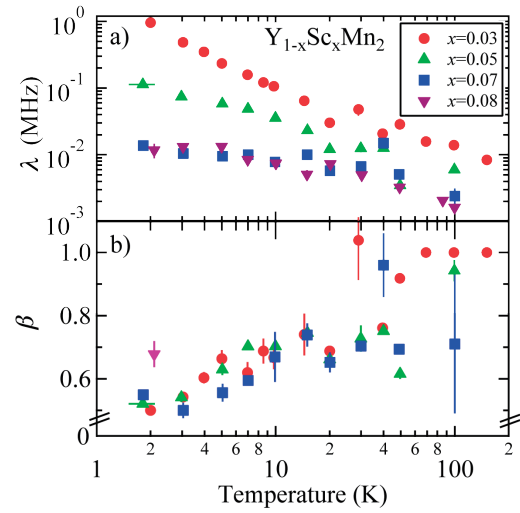


Fig. 5: Temperature dependences of (a) depolarization rate (λ) and power (β) for $\text{Y}(\text{Sc})\text{Mn}_2$ obtained by curve fitting of $A(t)$ for $x = 0.03$ (circles), 0.05 (triangles), 0.07 (squares), and 0.08 (inverted triangles). β for $x = 0.08$ is fixed at 2 K.

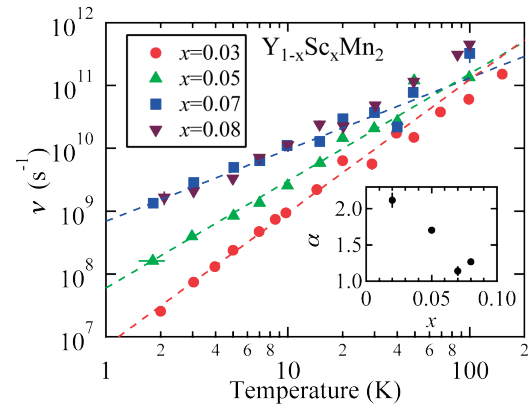


Fig. 6: Spin fluctuation rate (ν) as a function of temperature and Sc content (x) in $\text{Y}(\text{Sc})\text{Mn}_2$. Solid lines are the results of curve fitting using a power law ($\nu \propto T^\alpha$). Inset: α obtained by curve fitting vs x .

the samples with $x \geq 0.07$ is in the range of 10^9 – 10^{11} s^{-1} for $T \leq T^*$, while it shows a steeper reduction with decreasing temperature in those with $x \leq 0.05$. Although the use of stretched exponential decay in Eq. (22) prevents ν from being simply interpreted as a mean when $\beta < 1$, ν serves as a “characteristic frequency” that describes the spin dynamics on the basis of Eq. (13) [20]. Solid lines are obtained by curve fitting using the power law

$$\nu = c \cdot T^\alpha, \quad (24)$$

with c and α being free parameters. As shown in the inset of Fig. 6, α exceeds 2 in the case of $x = 0.03$, whereas it approaches unity ($\alpha \rightarrow 1$) for $x \geq 0.07$.

Here, it is worth stressing that NMR and

inelastic neutron scattering (INS) studies on the paramagnetic phase of $Y(\text{Sc})\text{Mn}_2$ conducted thus far have mostly been concerned with the relatively high energy part of the spin dynamics, where they demonstrated the presence of antiferromagnetic (AF) correlation with a characteristic frequency scale of $\nu_{\text{AF}} \approx 10^{13}\text{--}10^{14} \text{ s}^{-1}$ [21–25]. In particular, a strong hyperfine field exerted on ^{55}Mn nuclei [corresponding to $\delta_{\mu}^{\parallel}/\sqrt{2} \approx 1.2 \text{ GHz}/\mu_{\text{B}}$ in Eq. (13)] drives the sensitive range of NMR up to such high frequencies [23]. Interestingly, the latest INS study of a single-crystalline sample ($x = 0.03$) revealed that the intensity centered at approximately $Q_0 = (1.25, 1.25, 0)$ (in reciprocal lattice units) exhibits anisotropic broadening along the Brillouin zone boundary, which is interpreted to be due to the degeneracy of states associated with geometrical frustration [25]. Although this might be reminiscent of short-range correlations at a low energy, as similarly reported recently for LiV_2O_4 [26], the details are yet to be clarified.

2-3-2 $\text{YMn}_2\text{Zn}_{20-x}\text{In}_x$

One of the bottlenecks in the investigation of the d -electron HF state has been the limited number of candidate compounds that exhibit bulk electronic properties attributable to heavy-QP formation. Recently, it has been reported that a ternary intermetallic compound, $\text{YMn}_2\text{Zn}_{20}$, exhibits a large Sommerfeld coefficient ($\gamma \geq 200 \text{ mJ}\cdot\text{K}^{-2}\text{mol}^{-1}$) characteristic to the HF compounds [27, 28]. It crystallizes in the cubic $\text{CeCr}_2\text{Al}_{20}$ structure with the space group of $Fd\bar{3}m$ (see Fig. 7), where the Y and Mn atoms respectively occupy the $8a$ and $16d$ sites, forming diamond and pyrochlore lattices that are common to the cubic Laves phase $Y(\text{Sc})\text{Mn}_2$. Meanwhile, Zn atoms at the $16c$, $48f$, and $96g$ sites are located between the other two atoms, so that the pyrochlore lattice composed of the Mn atoms is almost doubly expanded in comparison with that in $Y(\text{Sc})\text{Mn}_2$ while keeping the tetrahedral symmetry. Although the compound with this ideal composition has not yet been obtained, the partial substitution of In for Zn is known to be effective for stabilizing the structure.

We have investigated the spin dynamics of Mn d -electrons by μSR under a zero/longitudinal field (ZF/LF) in a sample whose chemical composition is more precisely expressed as $\text{YMn}_{2+\delta}\text{Zn}_{20-15-x}\text{In}_x$ with $x=2.36$ [6], where the

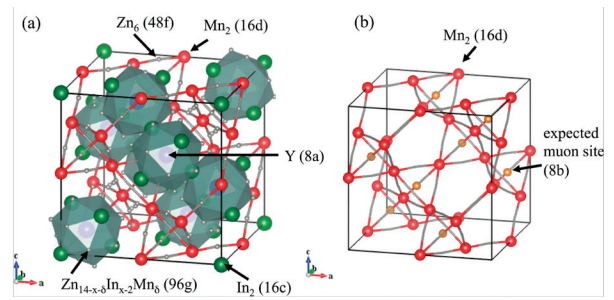


Fig. 7: (a) Crystal structure of $\text{YMn}_{2+\delta}\text{Zn}_{20-\delta-x}\text{In}_x$, where Y, Mn, Zn, and In atoms are indicated by blue, red, white, and green spheres, respectively. The Zn at the $96g$ site is partially substituted by In to stabilize the $\text{CeCr}_2\text{Al}_{20}$ structure. The actual compound exhibits a small amount (δ) of excess Mn that occupies the $96g$ site, where it substitutes for Zn. The Mn-Zn tetrahedra form a network similar to the pyrochlore lattice, where the local interaction between Mn atoms is relatively weaker than that in $Y(\text{Sc})\text{Mn}_2$ owing to the Zn atoms situated between the Mn atoms. (b) Expected muon site at the center of the Mn tetrahedra ($8b$ site) is shown.

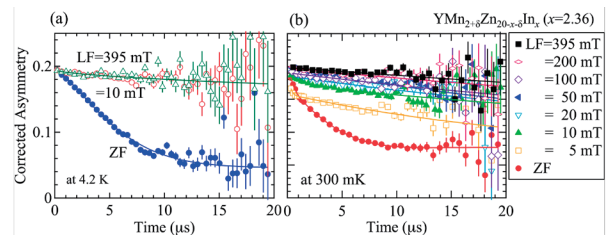


Fig. 8: ZF/LF- μSR time spectra of $\text{YMn}_{2+\delta}\text{Zn}_{20-\delta-x}\text{In}_x$ with $x=2.36$ ($\delta=0.11$) measured at (a) 4.2 K and (b) 300 mK. Solid curves are best fits using Eq. (22). The asymmetry of the spectrum under an LF of $B_0 = 395 \text{ mT}$ at 4.2 K is adjusted for comparison with the spectrum under an LF of $B_0 = 10 \text{ mT}$.

influence of excess Mn appears to be minimal [$\delta = 0.11(1)$] [28]. The sample was a mosaic of single crystals glued with varnish on a sample holder made of high-purity silver ($12\text{mm}\phi$ disc). μSR measurements in the range of 300–4.2 K (using a ^4He cryostat) were performed under an LF ($B_0 = 10 \text{ mT}$) to quench the depolarization due to random local fields from nuclear magnetic moments. Those in the range of 50 K–0.3 mK (with a ^3He cryostat) were performed under an LF ($B_0 = 395 \text{ mT}$) to distinguish depolarization due to the pyrochlore (on-site) Mn from that due to the excess Mn, where the yield of these signals was estimated from the field dependence of the LF- μSR spectra at 0.3 K.

Typical examples of ZF/LF- μSR spectra obtained at 4.2 and 0.3 K are shown in Fig. 8. The depolarization rate at 4.2 K is mostly independent

of B_0 (λ is unchanged between 10 and 395 mT), indicating that the spectra are in the limit of motional narrowing. These spectra were analyzed by curve fitting using Eq. (22), where $\beta = 1$ and a_p was replaced with A_b as the time-independent background mainly originating from muons stopped in the sample holder. The signal-to-background ratio (A_0/A_b) was ~ 3.8 for the ^4He cryostat and ~ 3 for the ^3He cryostat over a time range of 0–20 μs , allowing the reliable deduction of λ at small values ($\sim 10^{-2}\mu\text{s}^{-1}$).

While we have successfully estimated the contribution of on-site Mn from the total magnetic susceptibility assuming two components of the Curie–Weiss term with one ($\chi_{\delta \rightarrow 0}$) corresponding to the limit of $\delta = 0$ [28], it is often difficult to identify the contributions of the magnetic ions in question among those from impurities that also exhibit Curie–Weiss-like behavior. The true contribution of the on-site Mn was confirmed by muon Knight shift measurements [29], as was the case for $\text{Y}(\text{Sc})\text{Mn}_2$. The HTF- μSR spectra showed two frequency components with relative intensities of approximately 7 to 3, which was consistent with the values indicated from the partial asymmetries of the corresponding components in the LF- μSR spectra. The time spectra were then analyzed by curve fitting using Eq. (19) assuming two components.

The muon Knight shift (K_i) for each signal was obtained by Eq. (20) ($m = 2$), where the ratio of the signal amplitudes was consistent with that observed in the ZF/LF- μSR spectra, in which the contributions of the pyrochlore (on-site) and excess Mn were readily identified. This allowed us to unambiguously attribute the signal K_i to the intrinsic pyrochlore Mn. Curve fitting by the Curie–Weiss law yielded $|C| = 0.0036(3)$ emu·K/mol and $\theta_w = 13(2)\text{K}$, which showed nearly perfect agreement with $\chi_{\delta \rightarrow 0}$ in the temperature dependence. Consequently, as shown in Fig. 9, the K_i versus $\chi_{\delta \rightarrow 0}$ plot exhibited a linear relationship with $dK_i/d\chi_{\delta \rightarrow 0} = -13.1(6)$ MHz/ μ_B with a small offset of $K_0 = 13.5(4)$ ppm, indicating that $\chi_{\delta \rightarrow 0}$ indeed originated from the on-site Mn. Meanwhile, assuming that muons are located at the centers of Mn tetrahedra [8b site, shown in Fig. 7(b)], δ_μ^{\parallel} is calculated using the dipolar tensor for the Mn spins situated at the nearest- and next-nearest-neighboring tetrahedra to yield $|\delta_\mu^{\parallel}| = 2\pi \times 2.65$ MHz/ μ_B , which is in reasonable agreement with the experimental value.

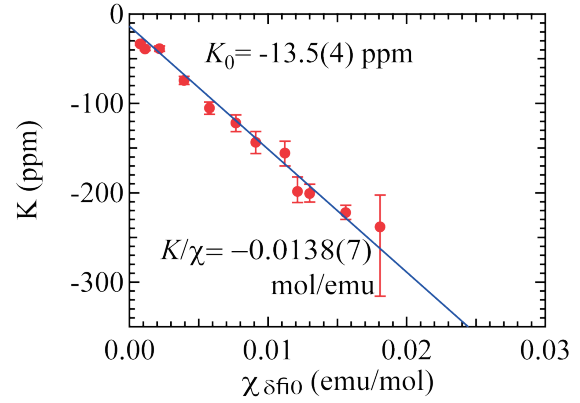


Fig. 9: Muon Knight shift (K_i) versus magnetic susceptibility ($\chi_{\delta \rightarrow 0}$) for intrinsic pyrochlore Mn in $\text{YMn}_{2+\delta}\text{Zn}_{20-\delta-x}\text{In}_x$.

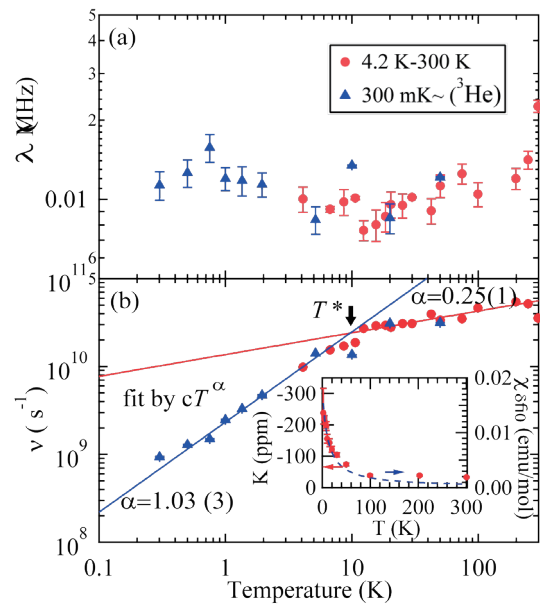


Fig. 10: Temperature dependence of (a) longitudinal spin relaxation rate (λ) and (b) spin fluctuation rate (ν) in $\text{YMn}_{2+\delta}\text{Zn}_{20-\delta-x}\text{In}_x$ with $x = 2.36$ ($\delta = 0.11$). The solid curves in (b) are results of least-squares fitting using a power law ($\nu \propto T^\alpha$) for the range of temperatures above and below T^* .

The potential influence of excess Mn can be avoided by employing values of λ obtained from data under an LF with magnitude greater than 100 mT. As shown in Fig. 10(a), λ tends to level off ($\lambda \propto T^0$) for $T \leq T^*$, which strongly resembles the case of $\text{Y}(\text{Sc})\text{Mn}_2$ with $x \geq 0.07$. Combining this result with $\chi_{\delta \rightarrow 0}$ and δ_μ , we obtain ν vs T using Eq. (13) as shown in Fig. 10(b). The linear temperature dependence of ν emerges below $T^* \sim 10\text{K}$, confirming our previous result [6] with improved reliability. Curve fitting using the power law [Eq. (24)] yields $\alpha = 1.03(3)$ [29], which is again consistent with the case of $\text{Y}(\text{Sc})\text{Mn}_2$. It is noticeable that ν exhibits a clear kink around $T^* \simeq 10\text{K}$,

below which ν becomes linearly dependent on T . Thus, T^* may be regarded as a crossover temperature below which the spin fluctuation is predominantly determined by the mechanism common to $\text{Y}(\text{Sc})\text{Mn}_2$.

We also note that $\lambda_{\perp}^{(1)}$ (the depolarization rate of the signal corresponding to the on-site Mn under a transverse field) was in the range of 1–2 MHz below ~ 30 K which was much greater than that expected from the magnitude of λ [≤ 0.02 MHz, see Fig. 10(a)], indicating the presence of additional line broadening due to the spin fluctuation associated with geometrical frustration in χ_{local} , as is also observed in $\text{Y}(\text{Sc})\text{Mn}_2$ and LiV_2O_4 .

2-3-3 LiV_2O_4

Lithium vanadate is the only compound that exhibits HF behavior among the numerous metal oxides so far studied, and therefore it has attracted much attention since its discovery in the late '90s. [3, 4] The formation of a heavy-QP state below a characteristic temperature ($T_K \approx 20$ – 30 K) is suggested by its large Sommerfeld coefficient ($\gamma \approx 420$ mJ/mol·K²) and other bulk properties that are hallmarks of typical f -electron HF compounds. Moreover, it has been inferred from the result of recent photoemission spectroscopy examination that a DOS peak slightly above E_F develops for $T < T_K$. [30]

In our previous μSR study, we showed using a powder specimen of LiV_2O_4 that the observed μSR spectra consisted of two components that could be distinguished by the response of the depolarization rate to an external magnetic field (B_0). [7] Furthermore, the component that exhibited the weaker dependence on B_0 (with longitudinal spin relaxation rate λ_D and fractional yield $f \approx 0.4$) was mostly independent of temperature below $T^* \sim 10^2$ K, from which we suggested that the corresponding fluctuation rate derived from the Redfield theory for the *local* spin systems was also independent of temperature ($\nu_D > 10^9$ s⁻¹). In contrast, the depolarization rate associated with the other signal (λ_S , with $1-f \approx 0.6$) was readily suppressed by B_0 , which was ascribed to slowly fluctuating local magnetic moments ($\nu_S \sim 10^6$ – 10^7 s⁻¹). Although the occurrence of such phase separation was confirmed by a subsequent μSR study of high-quality single-crystalline samples, the increased yield ($f \approx 0.8$) implied that clarifying the origin of ν_D was essential to our understanding of

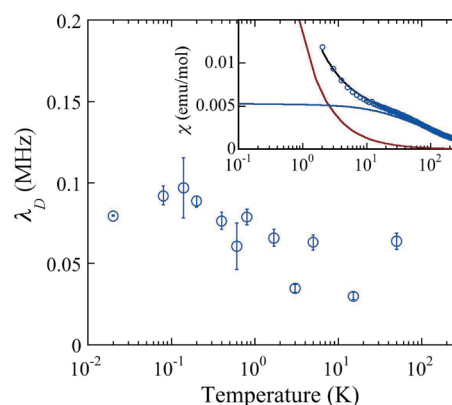


Fig. 11: Muon depolarization rate in LiV_2O_4 reproduced using data in Ref. [7] for the component showing fast fluctuation (ν_D). Inset: Temperature (T) dependence of χ with T having a logarithmic scale. Solid curves are results of curve fitting assuming two components, where the curve approaching 0.005 emu/mol is attributed to the intrinsic contribution of V (χ_V , see text for more details).

the electronic state. [10]

Figure 11 shows the muon depolarization rate (λ_D) under a zero external field, deduced by curve fitting using the sum of two components with exponential damping: [7]

$$G_z(t) = f \exp(-\lambda_D t) + (1-f) \exp(-\lambda_S t)$$

Although the data are scarce, particularly at higher temperatures, λ_D is only weakly dependent on temperature with a tendency to level off with decreasing temperature, which is qualitatively similar to the behavior of χ_V (Fig. 11, inset). These features are remarkably similar to those observed for $\text{Y}(\text{Sc})\text{Mn}_2$ ($x \geq 0.07$) and $\text{YMn}_2\text{Zn}_{20-x}\text{In}_x$.

A more appropriate evaluation of ν_D from λ_D using Eq. (13) for an itinerant system was recently carried out. [8] Since the muon Knight shift data obtained from the previous μSR measurement were not sufficient to evaluate the temperature dependence of K_i for the relevant component (particularly at low temperatures), [7] we extracted it from the bulk susceptibility (χ). More specifically, considering the behavior of χ observed in single-crystalline samples, which tends to saturate at lower temperatures [4, 31] we attributed the divergent behavior of χ at $T \rightarrow 0$ to unknown paramagnetic impurities (obeying the Curie law) and decomposed the data into two parts:

$$\begin{aligned} \chi &= \chi_V + \chi_{\text{imp}} \\ &= \frac{C_V}{T - \theta_W} + \frac{C_{\text{imp}}}{T}, \end{aligned} \quad (25)$$

where θ_W is the Weiss temperature. Curve fitting using Eq. (25) yielded $C_V = 0.387(5)$ emu·K/mol,

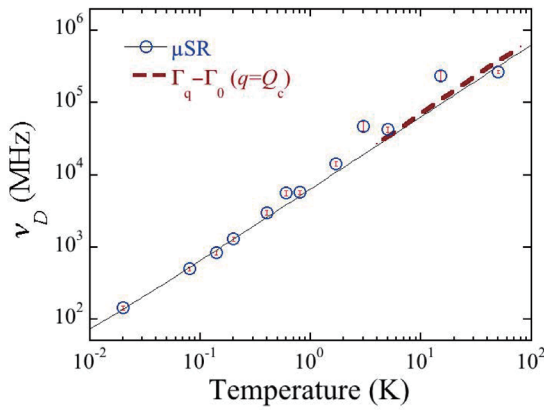


Fig. 12: Spin fluctuation rate (ν) in LiV_2O_4 as a function of temperature. The thin solid line shows a linear T dependence ($\nu \propto T$). Inelastic neutron scattering data are also shown for comparison, where the dashed curve shows the linewidth $(\Gamma_q - \Gamma_0)/h$ at $Q_c = 0.64 \text{ \AA}^{-1}$ with $\Gamma_0 \approx 1.5 \text{ meV}$. [32]

$\theta_W = -74(2) \text{ K}$, and $C_{\text{imp}} = 0.0131(2) \text{ emu}\cdot\text{K}/\text{mol}$, implying that the behavior of χ_V was in good agreement with that of single crystals [thus, we use $\chi = \chi_V$ in Eq. (13)]. Assuming that the Curie term originates from free V spins ($V^{3.5+} \sim 1.5\mu_B$), the fractional yield of the impurity phase estimated as C_{imp}/T was 1.6% of the total volume. This was much smaller than that of primary μSR signals (either f or $1 - f$ with $f \approx 0.4$), indicating that the paramagnetism of the impurity phase was irrelevant to the interpretation of μSR data.

Another important quantity in Eq. (13) is δ_{μ}^{\parallel} . The muon Knight shift measurements of both powder and single-crystalline samples yielded $\delta_{\mu(D)}^{\parallel} \approx 0.5 \pm 0.2 \text{ GHz}/\mu_B$, which corresponds to the component from which ν_D was deduced. [7, 10] Apart from the large error due to the broad linewidth, this $\delta_{\mu(D)}^{\parallel}$ was in good agreement with the calculated $\delta_{\mu(D)}^{\parallel}$ of $0.143 \text{ GHz}/\mu_B$ for muons that occupy a site at the center of a cyclic vanadium hexamer (as inferred from the observed μSR linewidth due to nuclear magnetic moments at high temperatures) and are subject to the magnetic dipolar fields from vanadium ions. [7] Since the experimental value of the hyperfine parameter had a large uncertainty due to the broad linewidth, we used the calculated value for the evaluation of ν_D [8].

The reevaluated ν_D is plotted in Fig. 12 together with INS data, [32] where one can observe that ν_D lies on a straight line, indicating its proportional relationship with temperature ($\nu_D \propto T$) over a T range of three decades below T^* . This is again strikingly similar to the behavior of the

spin fluctuation rate observed in $\text{Y}(\text{Sc})\text{Mn}_2$ and $\text{YMn}_2\text{Zn}_{20-x}\text{In}_x$ at lower temperatures ($T < T^*$). We also note that the corresponding low-energy excitation (also suggested in an earlier neutron scattering study [33]) has been confirmed by a recent INS experiment on high-quality samples [26].

2-4 Discussion

2-4-1 Spin fluctuation rate

As mentioned earlier, the heavy QP mass is phenomenologically understood to originate from the sharp increase in the DOS slightly above the Fermi level and the associated flattening of the band dispersion, i.e., $D(E_F) \propto (m^*)^{\sigma} \rightarrow \infty$ (with σ determined by the dispersion relation of electrons). In rare-earth compounds, such enhancement is induced by the conversion of local f -electron degrees of freedom into $D(E)$ by the Kondo effect, which is observed as a peak structure of $D(E)$ near E_F . The observation of such a structure ($\sim 4 \text{ meV}$ above E_F) in LiV_2O_4 by photoemission spectroscopy [30] appears to favor the Kondo mechanism established for f -electron compounds as a common microscopic origin of the HF behavior in the relevant compounds. However, further attempts to obtain support for this scenario have been elusive. A theoretical model to project d -electron states (1.5 electrons per $V^{3.5+}$ ion) onto the Kondo model by splitting them into two subbands by electronic correlation had to introduce an unusually large Kondo coupling ($J_K \sim 10^3 \text{ K}$) to overcome the competing effect of Hund coupling. [34, 35] Our μSR study of a single-crystalline sample provided evidence against the formation of a spin-singlet state as it showed the presence of the local vanadium moments at low temperatures far below $T^* \approx T_K$ (interpreted as the Kondo temperature), where the “local” spins would disappear in this scenario. [7, 10] From this view point, the importance of a highly symmetric crystal structure and the potential influence of geometrical frustration have been stressed by various authors, leading to a wide variety of theoretical models. [36-45]

The coexistence of slowly fluctuating local moments with the heavy-QP state at low temperatures in $\text{Y}(\text{Sc})\text{Mn}_2$ and $\text{YMn}_2\text{Zn}_{20-x}\text{In}_x$ supports the above-mentioned argument for LiV_2O_4 . The presence of local moments over the relatively long time range of $\nu^{-1} \approx 10^{-11} - 10^{-9} \text{ s}$ indicates that the conventional Kondo coupling (which virtually

eliminates local spins over a time scale longer than $\nu_{\text{ex}}^{-1} = h/J_{\text{cf}} \sim 10^{-14} - 10^{-13}$ s, where J_{cf} is the exchange energy between conduction electrons and f electrons) is not in effect, thereby suggesting a different origin of the heavy-QP state in these compounds.

According to a theoretical investigation of intersecting Hubbard chains as a model of the pyrochlore sublattice in LiV_2O_4 , the low-energy part of the spin dynamics is predicted to be described by a spin-spin correlation whose relaxation rate is proportional to temperature [46]. The behavior

$$\nu \propto T, \quad (26)$$

which is commonly observed in LiV_2O_4 , $\text{Y}(\text{Sc})\text{Mn}_2$ ($x \geq 0.07$, where the system is far from the spin-glass instability), and $\text{YMn}_2\text{Zn}_{20-x}\text{In}_x$ at lower temperatures, is perfectly consistent with the above prediction, suggesting that the t_{2g} orbitals associated with Mn/V atoms retain their 1D character at low temperatures (energies). In particular, the spin fluctuation rate (ν_D) in LiV_2O_4 deduced from μSR is perfectly in line with the relaxation rate ($\Gamma_Q \propto T$ for $T < 10^2$ K) observed over the low-energy region of the INS spectrum [32]. This implies that both μSR (sensitive over $0 \leq |\mathbf{q}| \leq \sim 1 \text{ \AA}^{-1}$) and INS probe common parts of the spin fluctuation spectrum of LiV_2O_4 , suggesting that a similar situation is realized for $\text{Y}(\text{Sc})\text{Mn}_2$ and $\text{YMn}_2\text{Zn}_{20-x}\text{In}_x$. Phenomenologically, this may be interpreted to mean that the heavy QPs develop in the manner $D(E_F) \propto (m^*)^\sigma \propto 1/T$ at lower temperatures.

Among the many theoretical models for the microscopic origin of the HF state in LiV_2O_4 , that proposed by Fujimoto regards the quasi-1D character of the t_{2g} bands associated with the pyrochlore lattice (consisting of intersecting chains of t_{2g} orbitals) as an essential basis for the description of the electronic state as it is expected that the hybridization between the 1D bands will be strongly suppressed owing to the geometrical configuration (frustration) [40]. This model incorporates the hybridization as a perturbation to the 1D Hubbard bands, which yields an energy scale (T^*) that characterizes the crossover from 1D to 3D as the Fermi liquid state develops with decreasing temperature below T^* . The calculated specific heat coefficient taking account of the latter as the leading correction to the self-energy yields a large value that is consistent with the experimentally observed values. The progression of hybridization

also induces the enhancement of the 3D-like spin correlation, which should appear as the enhancement of uniform susceptibility for $T < T^*$, while the spin fluctuation is dominated by the staggered component of 1D Hubbard chains.

2-4-2 Anomalous broadening of TF- μSR Spectra

Here we discuss the origin of the strong broadening of the TF- μSR linewidth observed in $\text{Y}(\text{Sc})\text{Mn}_2$ at lower temperatures ($T < T^*$), which is also expected to be relevant to the other two compounds. Since the muon site has a $\bar{3}m$ point symmetry for the cubic $Fd\bar{3}m$ structure, the presumed muon site suggests a powder pattern for $P(\omega)$ that is characterized by two singularities (edges) at ω_\perp and ω_\parallel due to the uniaxially anisotropic dipolar fields [47],

$$P(\omega) = \frac{1}{2\sqrt{(\omega - \omega_\perp)(\omega_\parallel - \omega_\perp)}}, \quad (27)$$

(see the inset of Fig. 13). Accordingly, we attempt to reproduce TF- μSR time spectra by curve fitting using the following form:

$$G_x(t) = \exp[-(\sigma t)^\beta] \int_{\omega_\parallel}^{\omega_\perp} P(\omega_\mu) \cos(\omega_\mu t + \phi_0) d\omega_\mu, \quad (28)$$

where stretched exponential damping was incorporated to consider the additional line broadening due to spin fluctuation.

Figure 13 shows result of such curve fitting for a time spectrum obtained at 2 K in the time domain with the inset showing the calculated $P(\omega)$ for (i) isotropic local spin susceptibility (black dotted curve) and (ii) assuming in-plane anisotropy (blue dashed curve), where the Mn moments are allowed to fluctuate within the easy plane perpendicular to the threefold rotation-inversion axis on the Mn site (which is parallel to the [111] direction). The latter means that the local spin susceptibility probed by a muon strongly depends on the field direction. Then, the local spin susceptibility becomes considerably greater than the isotropic case when the external field is parallel to the principal axis, and thereby χ in Eq. (18) should be replaced with the anisotropic χ_{local} (thus enhancing λ_\perp). The main panel of Fig. 13 shows the corresponding $A(t) = A_0 G_x(t)$ (black dotted and blue broken curves) calculated for the respective $P(\omega)$ using the parameters A_0 , λ , β , and ϕ_0 obtained from the curve fitting using Eq. (28). One can

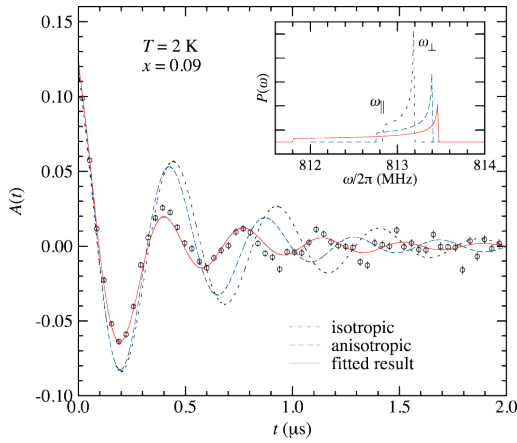


Fig. 13: Time dependent μ SR spectra for $Y_{1-x}Sc_xMn_2$ with $x = 0.09$ obtained at 2 K under a transverse field of 6 T. Dotted and broken curves are those calculated using $P(\omega)$ shown in the inset respectively assuming isotropic and anisotropic local spin susceptibility (see text for more details), and solid curves show the result of curve fitting with the uniaxial $P(\omega)$ plus additional line broadening. The data points and curves are displayed on a rotating reference frame with a frequency of 811 MHz.

observe that the spectrum is not reproduced by the two types of calculated curve and that further broadening is required. This clearly indicates the occurrence of excess line broadening, which is not explained by the anisotropy of the Knight shift.

We note that a similar result was obtained for the TF- μ SR time spectra in LiV_2O_4 . [10] In order to get more insight into this issue, we recently performed TF- μ SR measurements for newly synthesized single-crystalline LiV_2O_4 , and found that λ_{\perp} (corresponding λ_D under a longitudinal field) is strongly enhanced by increasing the external field (B_{TF}). [48] As shown in Fig. 14, λ_{\perp} exhibits monotonous increase in proportion to B_{TF} , where the value linearly extrapolated to 1.0T [= 2.43(9) MHz] is in perfect agreement with that previously observed. [10] We also examined the existing data for $Y_{1-x}Sc_xMn_2$ to find a similar trend, as inferred from the data at 30 K. These observations suggest the occurrence of a field-induced staggered magnetism in accordance with the slowing down of spin fluctuation. Considering Eq. (18) with the situation $\nu \gg \omega_{\mu}$ for the relevant field range, the field-induced effect must have a strong uniaxial anisotropy along with the field orientation to yield the relation $(\delta_{\mu}^{\perp})^2 > (\delta_{\mu}^{\parallel})^2$. This is understood by taking account of the fact that the Zeeman energy for a free electron spin is comparable to that corresponding to the spin fluctuation rate under a relevant magnetic field (10^{-2} – 10^0 meV). It is then

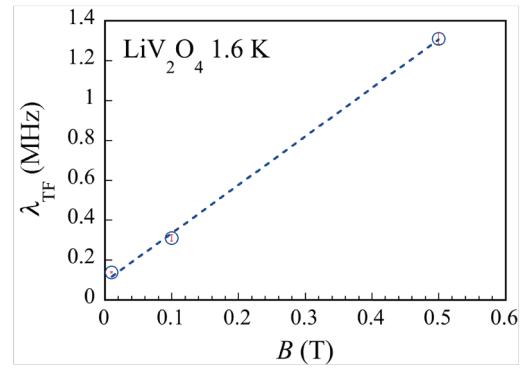


Fig. 14: Field dependence of the TF- μ SR line width in sc- LiV_2O_4 at 1.6 K.

likely that the external field would tend to suppress the spin fluctuation perpendicular to the field, while it leads to the increase of the mean value for the parallel component.

Thus, the increase in λ_{\perp} for $T < T^*$ is a common trait in $Y(Sc)Mn_2$, $YMn_2Zn_{20-x}In_x$, and LiV_2O_4 , and it is expected to be an important clue to understanding the HF-like behavior of these pyrochlore antiferromagnets in terms of spin fluctuation.

2-5. Summary and Conclusion

We have shown that the longitudinal spin relaxation rate in the d -electron HF-like compounds commonly exhibits a tendency to level off, $\lambda = 1/T_1 \propto T^0$, below a characteristic temperature T^* . This implies that the spin fluctuation rate becomes linearly dependent on temperature, $\nu \propto T$, in these compounds for $T < T^*$. In particular, such behavior in LiV_2O_4 is consistent with the implications of INS experiments, providing a basis for the coherent understanding of the low-energy spin dynamics through the theoretical model of intersecting 1D Hubbard chains that simulates a pyrochlore lattice. The persistent quasi-1D spin dynamics coexists with the enhanced local susceptibility at lower temperatures ($T < T^*$), which is also common to two other d -electron HF systems, $Y(Sc)Mn_2$ and $YMn_2Zn_{20-x}In_x$. These observations strongly indicate that a geometrically constrained t_{2g} band is the primary requirement for the formation of heavy QPs, with the 1D-to-3D crossover as a possible mechanism of effective mass enhancement.

Acknowledgements

The results quoted in this review were achieved under collaborations with the

Geometrical Correlation Project members including T. Yamazaki, Y. Tabata, and H. Nakamura for $Y(\text{Sc})\text{Mn}_2$, Y. Okamoto and Z. Hiroi for $\text{YMn}_2\text{Zn}_{20-x}\text{In}_x$, and H. Ueda, C. Urano, S. Kondo, M. Nohara, H. Takagi, Y. Matsushita, and Y. Ueda for LiV_2O_4 . The author would like to thank M. Miyazaki, I. Yamauchi, M. Hiraishi, T. Masuda, A. Koda, H. Okabe, K. M. Kojima, K. Ohishi, I. Kawasaki, I. Watanabe, and W. Higemoto for their active involvement in μSR experiments. We also thank K. Tomiyasu, S. Fujimoto, H. Tsunetsugu, and Y. Kuramoto for helpful discussions. The work was partly supported by the Inter-University Research Program of Institute of Materials Structure Science, KEK (Proposal Nos. 2011A0011, 2012A0051, 2013A0089, 2014A0238).

References

- [1] H. Wada, M. Shiga, and Y. Nakamura, *Physica B* **161**, 197 (1989).
- [2] R. A. Fisher, R. Ballou, J. P. Emerson, E. Lelièvre-Berna, and N. E. Phillips, *Int. J. Mod. Phys. B* **7**, 830 (1993).
- [3] S. Kondo, D. C. Johnston, C. A. Swenson, F. Borsa, A. V. Mahajan, L. L. Miller, T. Gu, A. I. Goldman, M. B. Maple, D. A. Gajewski, E. J. Freeman, N. R. Dilley, R. P. Dickey, J. Merrin, K. Kojima, G. M. Luke, Y. J. Uemura, O. Chmaissem, and J. D. Jorgensen, *Phys. Rev. Lett.* **78**, 3729 (1997).
- [4] C. Urano, M. Nohara, S. Kondo, F. Sakai, H. Takagi, T. Shiraki, and T. Okubo, *Phys. Rev. Lett.* **85**, 1052 (2000).
- [5] M. Miyazaki, R. Kadono, M. Hiraishi, T. Masuda, A. Koda, K. M. Kojima, T. Yamazaki, Y. Tabata, and H. Nakamura, *J. Phys. Soc. Jpn.* **80**, 063707 (2011).
- [6] M. Miyazaki, R. Kadono, M. Hiraishi, I. Yamauchi, A. Koda, K. M. Kojima, I. Kawasaki, I. Watanabe, Y. Okamoto, and Z. Hiroi, *J. Phys.: Conf. Ser.* **551**, 012019 (2014).
- [7] Koda, R. Kadono, W. Higemoto, K. Ohishi, H. Ueda, C. Urano, S. Kondo, M. Nohara, and H. Takagi, *Phys. Rev. B* **69**, 012402 (2004).
- [8] R. Kadono, A. Koda, W. Higemoto, K. Ohishi, H. Ueda, C. Urano, S. Kondo, M. Nohara, and H. Takagi, *J. Phys. Soc. Jpn.* **81**, 014709 (2012).
- [9] This report is mostly based on our recent review paper by M. Miyazaki, Y. Yamauchi, and R. Kadono, *J. Phys. Soc. Jpn.*, in press.
- [10] Koda, R. Kadono, K. Ohishi, S. R. Saha, W. Higemoto, Y. Matsushita, and Y. Ueda, *J. Phys.: Condens. Matter* **17**, L257 (2005).
- [11] Yamauchi, M. Miyazaki, M. Hiraishi, A. Koda, K. M. Kojima, R. Kadono, and H. Nakamura, unpublished.
- [12] Schenck, *Muon Spin Rotation Spectroscopy: Principles and Applications in Solid State Physics* (Adam Hilger, Bristol, 1985) Vol. 125.
- [13] T. Moriya, *Prog. Theor. Phys.* **16**, 23 (1956); *Prog. Theor. Phys.* **16**, 641 (1956).
- [14] R. Ballou, J. Deportes, R. Lemaire, Y. Nakamura, and B. Ouladdiaf, *J. Magn. Magn. Mater.* **70**, 129 (1987).
- [15] H. Nakamura, H. Wada, K. Yoshimura, M. Shiga, Y. Nakamura, J. Sakurai, and Y. Komura, *J. Phys. F: Met. Phys.* **18**, 981 (1988).
- [16] See, for example, I. Yamauchi, M. Itoh, T. Yamauchi, J. Yamaura, and Y. Ueda, *J. Phys.: Conf. Ser.* **200**, 012234 (2010).
- [17] M. Mekata, T. Asano, H. Nakamura, M. Shiga, K. M. Kojima, G. M. Luke, A. Keren, W. D. Wu, M. Larkin, Y. J. Uemura, S. Dunsinger, and M. Gingras, *Phys. Rev. B* **61**, 4088 (2000).
- [18] Hartmann, R. Wäppling, K. Aggarwal, L. Asch, A. Kratzer, G. M. Kalvius, F. J. Litterst, A. Yaouanc, P. Dalmas de Réotier, B. Barbara, F. N. Gygax, B. Hitti, E. Lippelt, and A. Schenck, *Hyperfine Interact.* **64**, 711 (1990).
- [19] Fujiwara, K. Ichinose, H. Nagai, and A. Tsujimura, *J. Magn. Magn. Mater.* **70**, 184 (1987).
- [20] D. C. Johnston, S. H. Baek, X. Zong, F. Borsa, J. Schmalian, and S. Kondo, *Phys. Rev. Lett.* **95**, 176408 (2005).
- [21] M. Shiga, H. Wada, Y. Nakamura, J. Deportes, B. Ouladdiaf, and K. R. A. Ziebeck, *J. Phys. Soc. Jpn.* **57**, 3141 (1988).
- [22] H. Nakamura and M. Shiga, *J. Alloys Compd.* **326**, 157 (2001).
- [23] G.-q. Zheng, K. Nishikido, K. Ohonishi, Y. Kitaoka, K. Asayama, and R. Hauser, *Phys. Rev. B* **59**, 13973 (1999).
- [24] Deportes, B. Ouladdiaf, and K. R. A. Ziebeck, *J. Magn. Magn. Mater.* **70**, 14 (1987).
- [25] R. Ballou, E. Lelièvre-Berna, and B. Fåk, *Phys. Rev. Lett.* **76**, 2125 (1996).
- [26] Tomiyasu, K. Iwasa, H. Ueda, S. Niitaka, H. Takagi, S. Ohira-Kawamura, T. Kikuchi, Y. Inamura, K. Nakajima, and K. Yamada, *Phys. Rev. Lett.* **113**, 236402 (2014).
- [27] Y. Okamoto, T. Shimizu, J. Yamaura, Y. Kiuchi, and Z. Hiroi, *J. Phys. Soc. Jpn.* **79**, 093712 (2010).

- [28] Y. Okamoto, T. Shimizu, J. Yamaura, Y. Kiuchi, and Z. Hiroi, *J. Solid State Chem.* **191**, 246 (2012).
- [29] Miyazaki, R. Kadono, M. Hiraishi, I. Yamauchi, A. Koda, K. M. Kojima, I. Kawasaki, I. Watanabe, Y. Okamoto, and Z. Hiroi, unpublished.
- [30] Shimoyamada, S. Tsuda, K. Ishizaka, T. Kiss, T. Shimojima, T. Togashi, S. Watanabe, C. Q. Zhang, C. T. Chen, Y. Matsushita, H. Ueda, Y. Ueda, and S. Shin, *Phys. Rev. Lett.* **96**, 026403 (2006).
- [31] Y. Matsushita, H. Ueda, and Y. Ueda, *Nat. Mater.* **4**, 845 (2005).
- [32] S.-H. Lee, Y. Qiu, C. Broholm, Y. Ueda, and J. J. Rush, *Phys. Rev. Lett.* **86**, 5554 (2001).
- [33] P. Murani, A. Krimmel, J. R. Stewart, M. Smith, P. Strobel, A. Loidl, and A. Ibarra-Palos, *J. Phys.: Condens. Matter* **16**, S607 (2004).
- [34] V. I. Anisimov, M. A. Korotin, M. Zöfl, T. Pruschke, K. Le Hur, and T. M. Rice, *Phys. Rev. Lett.* **83**, 364 (1999).
- [35] H. Kusunose, S. Yotsuhashi, and K. Miyake, *Phys. Rev. B* **62**, 4403 (2000).
- [36] Lacroix, *Can. J. Phys.* **79**, 1469 (2001).
- [37] P. Fulde, A. N. Yaresko, A. A. Zvyagin, and Y. Grin, *Europhys. Lett.* **54**, 779 (2001).
- [38] Shannon, *Eur. Phys. J. B* **27**, 527 (2002).
- [39] S. Burdin, D. R. Grempel, and A. Georges, *Phys. Rev. B* **66**, 045111 (2002).
- [40] S. Fujimoto, *Phys. Rev. B* **65**, 155108 (2002).
- [41] J. Hopkinson and P. Coleman, *Phys. Rev. Lett.* **89**, 267201 (2002).
- [42] H. Tsunetsugu, *J. Phys. Soc. Jpn.* **71**, 1844 (2002).
- [43] Y. Yamashita and K. Ueda, *Phys. Rev. B* **67**, 195107 (2003).
- [44] M. S. Laad, L. Craco, and E. Müller-Hartmann, *Phys. Rev. B* **67**, 033105 (2003).
- [45] R. Arita, K. Held, A.V. Lukoyanov, and V. I. Anisimov, *Phys. Rev. Lett.* **98**, 166402 (2007).
- [46] J. D. Lee, *Phys. Rev. B* **67**, 153108 (2003).
- [47] See, for example, C. P. Slichter, *Principles of Magnetic Resonance*, 3rd Edition, (Springer-Verlag, New York, 1990).
- [48] H. Okabe, M. Hiraishi, A. Koda, K. M. Kojima, R. Kadono, and Y. Matsushita, to be published.